ELSEVIER

Journal of Alloys and Compounds 449 (2008) 339–342

Journal of ALLOYS AND COMPOUNDS

www.elsevier.com/locate/jallcom

Synthesis of Li_2MnO_3-like electrode materials by reaction in solutions

S.H. Kim [a], S.J. Kim [a], K.S. Nahm [b], H.T. Chung [c], Y.S. Lee [d], J. Kim [a,*]

[a] *Department of Materials Science and Engineering, Chonnam National University, Gwangju 500-757, South Korea*
[b] *Schoot of Chemical Engineering and Technology, Chonbuk National University, Jeonju 561-756, South Korea*
[c] *Department of Ceramic Engineering, Dongshin University, Naju 520-714, South Korea*
[d] *School of Applied Chemical Engineering, Chonnam National University, Gwangju 500-757, South Korea*

Received 4 November 2005; received in revised form 3 January 2006; accepted 10 January 2006
Available online 29 December 2006

Abstract

The nickel–manganese compounds were synthesized by redox reactions in aqueous solutions using potassium permanganate and nickel chloride at ambient temperature. Layered structured materials in Li–Ni–Mn–O system were synthesized by using the formed nickel–manganese compounds as a precursor for electrode materials to examine the electrochemical activity. X-ray diffraction patterns of the Li_2MnO_3-like $Li_{1.296}Ni_{0.056}Mn_{0.648}O_2$ sample were indexed to a layered structure based on hexagonal α-$NaFeO_2$ with a superlattice existence indicating a monoclinic Li_2MnO_3 crystalline phase. The electrode provides the initial discharge capacity of 108 mAh/g and the maximum discharge capacity of 192 mAh/g between 2.0 and 4.8 V versus Li/Li^+ at 0.2 mA/cm^2.

Keywords: Lithium batteries; Nickel–manganese; Redox reactions; Li_2MnO_3; Electrode

1. Introduction

A high firing temperature is required to overcome the diffusional limitations associated with limitations size of the reactant particles in solid-state reaction which are predominately used. Such a high-temperature procedure gives the larger particle size and inhomogeneity. These difficulties have prompted materials chemists to design and develop synthesis methods that can lower the processing temperatures [1,2]. Therefore, several low-temperature methods have attracted much attention in recent years in order to improve various kinds of performances [3–5]. Especially, the low-temperature methods lead to smaller and uniform particle size, which may be beneficial for electrodes materials development efforts in lithium batteries.

Layered lithium manganese oxides are of interest as an alternative cathode material due to their high specific energy, non-toxicity and low cost. Unfortunately, those layered manganese materials transform to the spinel-like phases by Jahn-Teller distortion during electrochemical cycling. This transformation usually leads to poor rate performance and to steps in the voltage profile [6–8]. To overcome this problem, a number of research groups have studied for increasing the structural stability of lithium manganese oxides by using a concept of a solid solution or nano-composite of $LiMO_2$ (M = Ni, Co, Cr) and Li_2MnO_3 [9–12]. Although whether the concept of a solid solution or a nano-composite formation for the $LiMO_2$–Li_2MnO_3 system is still in debate, $Li[Ni_xLi_{(1/3-2x/3)}Mn_{(2/3-x/3)}]O_2$ of them seems to be a promising candidate as cathodic material for lithium batteries. The $Li[Ni_xLi_{(1/3-2x/3)}Mn_{(2/3-x/3)}]O_2$ compounds exhibit the thermal stability and good electrochemical performance [13–15]. Lu et al. reported the layered $Li[Ni_xLi_{(1/3-2x/3)}Mn_{(2/3-x/3)}]O_2$ ($0 \le x \le 1/2$) compounds prepared by the "mixed hydroxide" method. $Li[Ni_xLi_{(1/3-2x/3)}Mn_{(2/3-x/3)}]O_2$ with $x = 1/3$ shows a capacity of 200 mAh/g at 30 °C and 220 mAh/g at 50 °C. Its good electrochemical performance is assumed that all Ni^{2+} is oxidized to Ni^{4+} when Li is extracted from $Li[Ni_xLi_{(1/3-2x/3)}Mn_{(2/3-x/3)}]O_2$ [13]. In relation to solid solution materials, Li_2MnO_3 has recently been researched for its unexpected electrochemical activity [16–19].

In this work, the nickel–manganese compounds were synthesized by redox reactions in aqueous solutions using potassium permanganate as oxidizing agents at ambient temperature. The prepared particles were used as a precursor for electrode mate-

* Corresponding author. Tel.: +82 62 530 1703; fax: +82 62 530 1699.
E-mail address: jaekook@chonnam.ac.kr (J. Kim).

0925-8388/$ – see front matter © 2006 Elsevier B.V. All rights reserved.
doi:10.1016/j.jallcom.2006.01.133

rials by lithiation with lithium hydroxide. It is particularly interesting to observe a stable electrochemical performance of $Li_{1.296}Ni_{0.056}Mn_{0.648}O_2$ material since it has almost identical stoichiometry and crystalline characteristics to Li_2MnO_3 which has been known as an electrochemically inactive material.

2. Experimental

The nickel–manganese compounds were synthesized by reacting an aqueous solution of nickel chloride with potassium permanganate. By using a burette a 50 mL aqueous solution of a 0.5 M $NiCl_2{\cdot}6H_2O$ and a 50 mL aqueous solution of a 0.5 M HCl were dropped slowly into 50 mL of a 0.5 M $KMnO_4$ solutions that was stirred constantly with a magnetic stirrer. The precipitate formed after 1 day of reaction was filtered, washed several times with distilled water to remove other reaction products. The precipitates were then dried in an oven at 100 °C for 6 h. To investigate the electrochemical activity of Li_2MnO_3, the as-prepared sample obtained by adding HCl was selected and lithiated. The as-prepared sample was mixed with the stoichiometric amount of $Li(OH){\cdot}2H_2O$ in accordance to the inductively coupled plasma (ICP) result of the sample, and ground. The mixture was pelletized and heated in air at 800 °C for 3 h and quenched to room temperature.

The crystalline nature and morphologies of the products were characterized by X-ray powder diffraction (XRD), and field emission scanning electron microscope (FESEM). The structural characterization of the synthesized samples was carried out with X-ray powder diffraction. The X-ray patterns were recorded with a counting degree of 2.00°/min in 2θ range from 10 to 80° by using a Rigaku D/MAX UltimaIII High Resolution X-ray Diffractometer (Cu Kα radiation). The morphology and particle size of the samples were characterized with S-4700 FESEM. The chemical composition of the as-prepared samples was determined by inductively coupled plasma using a Perkin-Elmer 4300 DV analyzer.

For electrochemical measurements, lithium-inserted materials were mixed with a carbon black and PTFE binder. This mixture were pressed onto a stainless steel mesh and dried under vacuum at 180 °C for 5 h. The cell consisted of a cathode and lithium metal anode separated by a glass fiber. The used electrolyte was a 1:1 mixture of ethylene carbonate (EC) and dimethyl carbonate (DMC) containing 1 M $LiPF_6$. The cells were assembled in a glove box under argon atmosphere and tested between 2.0 and 4.8 V versus Li/Li^+ at 0.2 mA/cm^2 by using Battery Tester System 2004.

3. Results and discussion

Fig. 1 shows the X-ray diffraction patterns of the samples obtained by reacting an aqueous solution of nickel chloride with potassium permanganate as oxidizing agent. The as-prepared samples show no discernible reflections in the X-ray powder diffraction pattern since those samples were synthesized by redox reactions in aqueous solutions at room temperature as shown in Fig. 1(a). To characterize the crystal structure, X-ray powder diffraction patterns were also recorded after firing at 500 °C for 6 h. The X-ray patterns of the fired sample shows the existence of the two phases corresponding to tetragonal α-MnO_2 and cubic Mn_2O_3 as shown in Fig. 1(b). The existence of the two phases in Fig. 1(b) was understood that the manganese oxides undergo structural and compositional changes as elevated temperatures ($T \sim 400$ °C) [20]. For example, γ-MnO_2 is decomposed to Mn_2O_3 at $T > 450$ °C [21]. Although any phases related to nickel was not found by X-ray diffraction patterns, the result of ICP shows the small amount of nickel was contained in the as-prepared sample showing transition metal chemistry of $Ni_{0.089}Mn_{1.034}$.

Fig. 2 shows the FESEM micrographs revealing the morphology of the samples. While the FESEM micrograph of the as-prepared sample shows that the as-prepared sample is in the form of spherical agglomerates, approximately 0.8–1.0 μm in diameter, the sample obtained by firing at 500 °C for 6 h has the smaller primary particles (<30 nm) with narrow particle

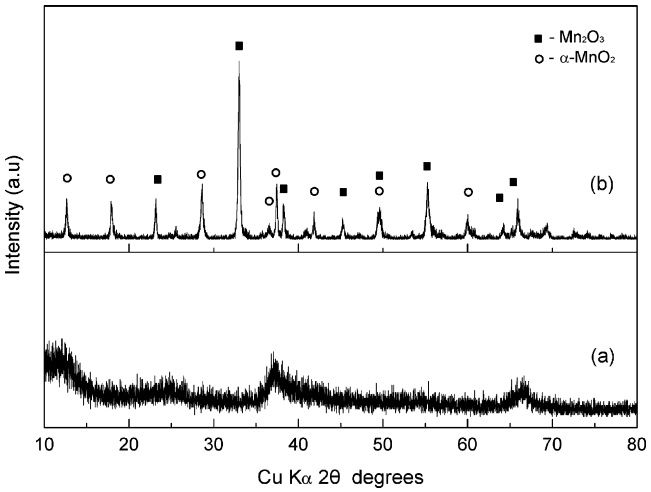

Fig. 1. The X-ray power diffraction patterns of: (a) the as-prepared sample and (b) after firing the sample at 500 °C for 6 h.

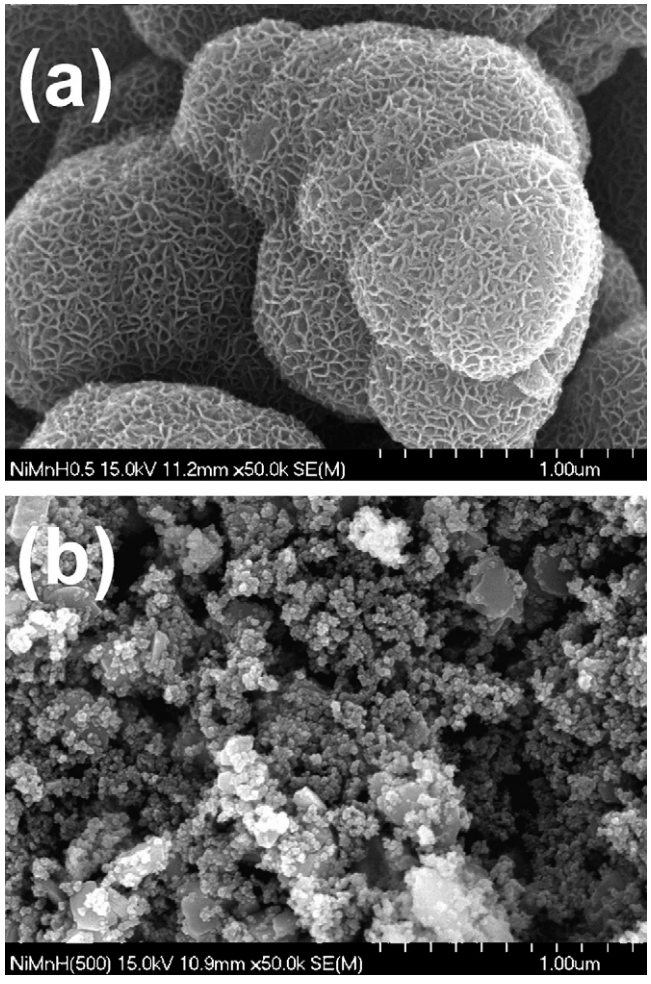

Fig. 2. The field emission SEM micrograph of: (a) the as-prepared sample and (b) after firing the sample at 500 °C for 6 h.

size distribution as shown in Fig. 2(a and b). The as-prepared sample exhibits loosely bonded agglomerates with very weak inter-particle bonding forces so that it readily decomposes to individual nanoparticles once enough activating treatments are induced.

Fig. 3 shows the X-ray powder diffraction patterns and the FESEM micrograph of the lithiated sample ($Li_{1.296}Ni_{0.056}Mn_{0.648}O_2$) prepared by quenching at 800 °C. The X-ray diffraction patterns of $Li_{1.296}Ni_{0.056}Mn_{0.648}O_2$ were indexed a layered structure based on hexagonal α-$NaFeO_2$ (space group: *R*-3*m*, 166), except for broad peaks between 20° and 25° as shown in Fig. 3(a). These broad peaks indicate the short-ranged superstructure ordering of the Li, Ni, and Mn atoms in the transition metal layers and indicating the presence of monoclinic Li_2MnO_3 phase [13,22]. Actually, $Li_{1.296}Ni_{0.056}Mn_{0.648}O_2$ material has a very similar stoichiometry to Li_2MnO_3 known as an electrochemically inactive materials. The morphology of the lithiated sample together with XRD results reveals that the particles are well crystallized. The particle size of the lithiated sample ($Li_{1.296}Ni_{0.056}Mn_{0.648}O_2$) is approximately 2–3 μm as shown in Fig. 3(b). It has been reported that manganese oxide has a substantially tendency for crystal growth with respect to a solid-state reaction at high temperature [23] resulting much larger particles than the samples heated at 500 °C as shown in Fig. 2.

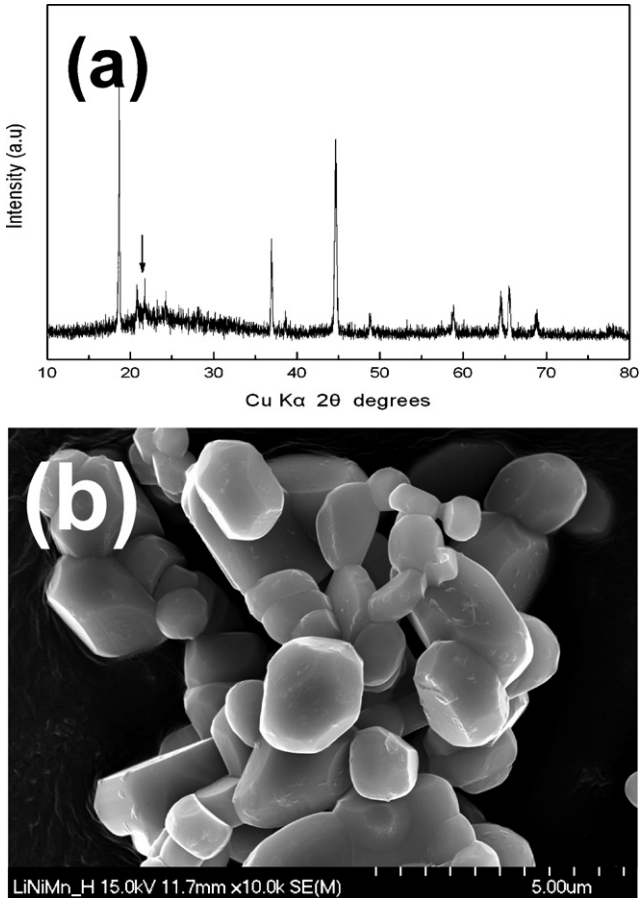

Fig. 3. (a and b) The X-ray powder diffraction patterns and the FESEM micrograph of the lithiated sample ($Li_{1.296}Ni_{0.056}Mn_{0.648}O_2$).

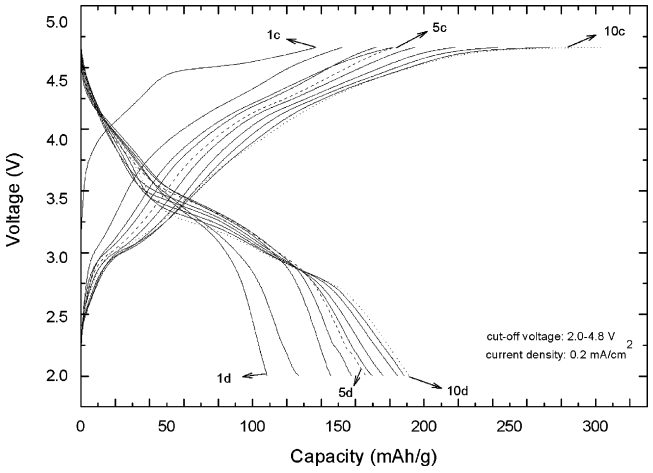

Fig. 4. Charge–discharge curves of Li/Li-inserted sample ($Li_{1.296}Ni_{0.056}Mn_{0.648}O_2$) cell in the voltage range of 2.0–4.8 V at a current density of 0.2 mA/cm^2.

Fig. 4 shows the charge–discharge curves of the lithiated sample A in the voltage range of 2.0–4.8 V at a current density of 0.2 mA/cm^2. It reveals that the voltage profile of the first charge cycle is very different from the others. There is a plateau at about 4.5 V during the first charge that leads to an increase in reversible capacity. Lu et al. reported that the voltage profile of the first charge up to 4.45 V is attributed to extraction of lithium by oxidation of Ni^{2+} to Ni^{4+}. The plateau at 4.5 V is related to the extraction of the remaining lithium from the lithium layer with accompanying the oxygen loss [14]. Recently, Shin and Manthiram reported that, if Li^+ ions could be removed from the host structure, Mn^{4+}-based samples could show a capacity by the hybridization of O^{2-}:2p and $Mn^{4+/5+}$:3d at higher voltage (>4.5 V) [24]. There is a irreversible capacity of about 30 mAh/g during the first charge–discharge as shown in Fig. 4. The electrochemical performance of the lithiated sample ($Li_{1.296}Ni_{0.056}Mn_{0.648}O_2$) shows the very interesting results that the discharge capacity continuously increases upon 1st to 10th cycles. The lithiated sample ($Li_{1.296}Ni_{0.056}Mn_{0.648}O_2$) exhibits a discharge capacity of 108 mAh/g at 1st cycle and a larger discharge capacity of 192 mAh/g at 10th cycle.

Fig. 5 shows the differential capacity versus voltage of Li/Li-inserted sample ($Li_{1.296}Ni_{0.056}Mn_{0.648}O_2$) cell in the voltage range of 2.0–4.8 V at a current density of 0.2 mA/cm^2. It shows that the differential capacity profile of the first charge cycle is different from the others. The peak at 3.3 V separates two peaks (2.8 V, 3.3 V) after 5th cycle. Wu et al. reported that the peak located at 3.3 V may be related to the reduction of Cr^{6+} to Cr^{3+} and Cr^{4+} to Cr^{3+}, while the peak located at 2.8 V may be attributed to the reduction of Mn^{4+} to Mn^{3+}, which results from the Mn-rich phase in the presence of less chromium [25]. Lu et al. reported that all the Ni is reduced to Ni^{2+} once the cells reach 3.5 V and Mn reduces continuously until the Li layers are occupied again below 3.5 V [14]. However, since $Li_{1.296}Ni_{0.056}Mn_{0.648}O_2$ material contains negligible amounts of nickel, it is unreasonable to consider any redox couples related to nickel for contributing the capacities at 2.8 and 3.3 V. Rather, it is assumed that both of the capacities at 3.3 and 2.8 V may

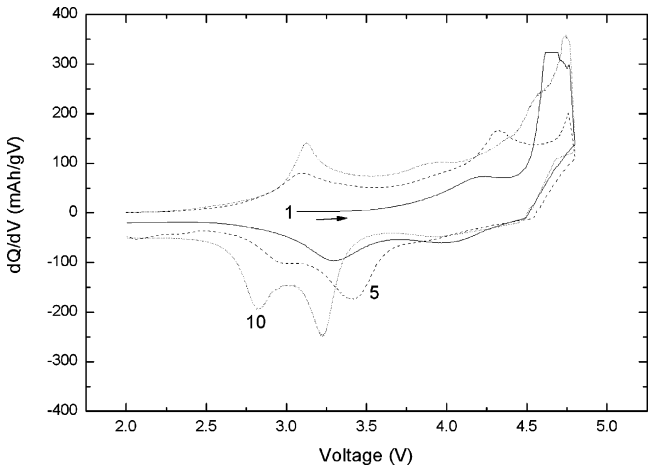

Fig. 5. The differential capacity vs. voltage of Li/Li-inserted sample ($Li_{1.296}Ni_{0.056}Mn_{0.648}O_2$) cell in the voltage range of 2.0–4.8 V at a current density of 0.2 mA/cm^2.

be attributed to Mn^{3+}/Mn^{4+} redox couple arising from Li insertion to tetrahedral and octahedral site in the materials which is partially transformed to spinel structures in discharging reactions. The lattice energies in specific sites, which directly affect work function values, are influenced by several factors such as Madelung constants, polarization effects, crystal field stabilization energy, etc. It is hard to state clearly at this stage regarding the origin of the capacities at 3.3 and 2.8 V. Therefore, a further study is necessary to understand the relationship between the potential and the material's structural information while cycling.

The curve also shows that the peak indicated the Li_2O extraction at higher voltage (>4.5 V) remains on cycling. This suggests that the continuous increase of capacity may be attributed to the remaining Li_2O after cycling. Shin et al. reported that the sufficient electrochemical inactive Li_2MnO_3 component contributes to stabilization of the Li–Ni–Mn–O structures. The discharge capacities of the $Li[Ni_xLi_{(1/3-2x/3)}Mn_{(2/3-x/3)}]O_2$ electrodes increase when the nickel content is small ($x \leq 0.275$), and then stabilize within about 20th cycles [15]. The increase of the peak height during cycling may be attributed to an increase in electrical contact between the particles of the cathode material [25]. Both the negative shift of the reduction peaks and the positive shift of the oxidation peaks seem to be related to the increase of the cell resistance.

4. Conclusions

The nickel–manganese compounds were synthesized by redox reactions in aqueous solutions at room temperature in acidic conditions. The selected as-prepared sample obtained by adding HCl was developed as a precursor for electrode materials to examine the electrochemical activity of Li_2MnO_3-like $Li_{1.296}Ni_{0.056}Mn_{0.648}O_2$. X-ray diffraction pattern of the lithiated sample ($Li_{1.296}Ni_{0.056}Mn_{0.648}O_2$) was indexed to a layered structure based on hexagonal α-$NaFeO_2$ with signs of superstructure existence indicating a monoclinic Li_2MnO_3 phase. The initial discharge capacity of the lithiated sample ($Li_{1.296}Ni_{0.056}Mn_{0.648}O_2$) continuously increases during electrochemical cycling. The lithiated sample ($Li_{1.296}Ni_{0.056}Mn_{0.648}O_2$) exhibits the maximum discharge capacity of 192 mAh/g on 10th cycle between 2.0 and 4.8 V at a current density of 0.2 mA/cm^2. Further study on the synthesis of nickel–manganese nanoparticles in optimized process conditions for precursor materials is being undertaken.

Acknowledgement

This work was supported by the Core Technology Development Program of the Ministry of Commerce, Industry and Energy (MOCIE).

References

[1] F.J. Disalvo, Science 247 (1990) 649;
J.B. Wiley, R.B. Kaner, Science 255 (1992) 1093;
A. Stein, S.W. Keller, T.E. Mallouk, Science 259 (1993) 1558.
[2] A. Manthiram, J. Kim, Chem. Mater. 10 (1998) 2895.
[3] J. Livage, M. Henry, C. Sanchez, Prog. Solid State Chem. 18 (1988) 259.
[4] A. Manthiram, J.B. Goodenough, Nature 329 (1987) 701.
[5] Y.F. Shen, R.P. Zerger, R.N. DeGuzman, S.L. Suib, L. Mccurdy, D.I. Potter, C.L. O'Young, Science 260 (1993) 511.
[6] R.J. Gummow, M.M. Thackeray, J. Electrochem. Soc. 140 (1993) 3365.
[7] Y. Shao-Horn, S.A. Hackeray, J. Electrochem. Soc. 146 (1999) 2404.
[8] Y.I. Jang, B. Huang, Y.M. Chiang, D.R. Sadoway, Electrochem. Solid-State Lett. 1 (1998) 13.
[9] Z.H. Lu, J.R. Dahn, J. Electrochem. Soc. 149 (2002) 815.
[10] Y. Shao-Horn, S.A. Hackney, A.R. Armstrony, P.G. Bruce, R. Gitzendanner, C.S. Johnson, M.M. Thackeray, J. Electrochem. Soc. 146 (1999) 2404.
[11] K. Numata, C. Sakaki, S. Yamanaka, Solid State Ionics. 117 (1999) 257.
[12] T. Ohzuku, Y. Makimura, Chem. Lett. (2001) 744.
[13] Z. Lu, D.D. MacNeil, J.R. Dhan, Electrochem. Solid-State Lett. 4 (11) (2001) 191.
[14] Z. Lu, L.Y. Beaulieu, R.A. Donaberger, C.L. Thomas, J.R. Dhan, J. Electrochem. Soc. 149 (2002) A778.
[15] S.-S. Shin, Y.–K. Sun, K. Amine, J. Power Sources 112 (2002) 634.
[16] A.D. Robertson, P.G. Bruce, Chem. Commun. 23 (2002) 2790.
[17] P. Kalyani, S. Chitra, T. Mohan, S.J. Gopukumar, J. Power Sources 80 (1999) 103.
[18] C.S. Johnson, J.-S. Kim, C. Lefief, N. Li, J.T. Vaughey, M.M. Thackeray, Electrochem. Commun. 6 (2004) 1085.
[19] C.S. Johnson, N. Li, J.T. Vaughey, S.A. Hackney, M.M. Thackeray, Electrochem. Commun. 7 (2005) 528.
[20] H. Ikeda, M. Hara, S. Narukawa, U.S. Pat. 4,133,856.(1979).
[21] C. Tsang, J. Kim, A. Manthiram, J. Solid State Chem. 137 (1998) 28.
[22] K.S. Kim, S.W. Lee, H.S. Moon, H.J. Kim, B.W. Cho, W.I. Cho, J.B. Choi, J.W. Park, J. Power Sources (2004).
[23] Z.P. Guo, S. Zhong, G.X. Wang, G. Walter, H.K. Liu, S.X. Dou, J. Electrochem. Soc. 149 (2002) A792.
[24] Y. Shin, A. Manthiram, Electrochim. Acta 48 (2003) 3583.
[25] X. Wu, K.S. Ryu, Y.S. Hong, Y.J. Park, S.H. Chang, J. Power Sources 132 (2004) 219.